FOURIER ANALYSIS OF AN INCOMPRESSIBLE FLOW SOLVER STABILIZED BY PRESSURE-GRADIENT PROJECTION

Gustavo C. Buscaglia[1], Fernando G. Basombrío[1] and Ramon Codina[2]
[1]Centro Atómico Bariloche and Instituto Balseiro, 8400 Bariloche, Argentina
[2] ETSCCP, Universitat Politècnica de Catalunya, Jordi Girona 1-3, Edifici C1, 08034 Barcelona, Spain

ABSTRACT

Fourier analysis techniques are applied to the stabilized finite element method recently proposed by Codina and Blasco for the approximation of the incompressible Navier-Stokes equations, here denoted by SPGP method (Stabilization by Pressure Gradient Projection). The analysis is motivated by spurious waves that pollute the computed pressure in start-up flows simulation. An example of this spurious phenomenon is reported. It is shown that Fourier techniques can predict the numerical behavior of stabilized methods with remarkable accuracy, even though the original Navier-Stokes setting must be significantly simplified to apply them. In the steady case good estimates for the stabilization parameters are obtained. In the transient case spurious long waves are shown to be persistent when the element Reynolds number is large and the Courant number is small. This can be avoided by treating the pressure gradient projection implicitly, though with additional computing effort. Standard extrapolation variants are unfortunately unstable. Comparisons to Galerkin-Least-Squares method and Chorin's projection method are also addressed.

INTRODUCTION

Much effort has been devoted in the last years to the development of finite element methods for incompressible flows allowing for identical interpolation for velocity and pressure unknowns to be used. It is well known that the usual Galerkin formulation violates the Babuška-Brezzi (BB) stability condition for such *equal-order* approximations, so that *stabilization* is needed. Several stabilized formulations have been developed over the years. Some of them, such as the popular GLS method,[10,11] explicitly perturb the Galerkin formulation by mesh dependent terms so as to improve stability. In other formulations, the stabilization terms are implicit within a fractional step algorithm. This is the case, for example, of projection methods based on the early ideas of Chorin.[3]
The equal-order method analysed in this article combines, in some sense, the two stabilization procedures mentioned above. An explicit stabilization term is incorporated that, in turn, mimics the effect of fractional step methods. To our knowledge, the first precedent of this method was proposed by Habashi *et al*[12] as the following modification of the zero-divergence constraint

$$div\ u - \lambda \nabla^2 p = -\lambda div\ g$$

where $g = \nabla p$ and λ is a small parameter. Though at the continuous level the terms containing λ cancel exactly, upon finite element discretization cancellation no longer occurs and these terms in fact stabilize the formulation. Equivalent terms in the finite element equations were later identified by Zienkiewicz and Codina[19] as explaining the

good behavior of an equal-order fractional step method. Finally, Codina and Blasco[6–8] formulated and analyzed theoretically an equal-order method based on these ideas. From the convergence analysis an elementwise estimate $\lambda \sim h^2$ (for h small) was derived, and optimal convergence rates obtained. We will refer to this method hereafter as SPGP (Stabilized by Pressure Gradient Projection). Recent work by Codina[5] has shown a link between this method and the Sub-Grid Scales method.[13]

The main drawback of the SPGP method is the introduction of the projection of the pressure gradient as a new unknown, thus increasing substantially the size of the final discrete system. However, iterative strategies may be devised to make the cost similar to that of other stabilized methods. On the other hand, when the transient Navier-Stokes equations are discretized using a finite difference scheme, the projection of the pressure gradient can be treated explicitly. In this case, the increase of cost is very low.

Many numerical tests have recently been performed to the SPGP method, involving steady and transient, two- and three-dimensional flows,[2,15] with quite good results. A turbulent code based on the SPGP method also exhibits good behavior.[16] Most of these tests deal with the pressure gradient projection explicitly. Comparing the SPGP and GLS methods, it was found that the former leads to better conditioning of the system matrix and smoother temporal behavior of the pressure field in transients. As drawback, spurious long-wave pressure transients in strongly accelerated flows (such as start-up flows) were detected. One of these cases is reported below. These spurious transients do not affect the velocity field, but render the pressure field useless until their extinction. Fortunately, no such phenomenon occurs in smooth flows (such as vortex shedding flows).

Summarizing, its overall performance makes the SPGP method attractive for equal-order finite element treatment of incompressible flows, mainly transient ones, and further work is needed to understand and improve its properties.

In this article Fourier analysis techniques are applied to the SPGP method and some of its variants. Several simplifications are introduced to render this analysis feasible: First, a one-dimensional model problem that mimics the Navier-Stokes equations is introduced and discretized. Second, the domain is assumed to be $(-\infty, +\infty)$, so that all nodes are equivalent. Finally, the convective nonlinear term is linearized. From the Fourier analysis of the discrete equations appropriate choices of stabilization coefficients are obtained. In the transient case stability is discussed. Moreover, a spurious oscillatory behavior is identified that explains 2D numerical results for start-up flow around a cylinder at Reynolds 3000. In particular, it is shown that the explicit treatment of the pressure-gradient projection activates this spurious behaviour and that a high-Reynolds stabilization coefficient improves the results. Comparisons to GLS and Chorin's methods are also addressed. Numerical results of the 1D model problem in a bounded domain without linearizing the convective term show that the conclusions from Fourier analysis apply in more realistic situations.

DESCRIPTION OF THE NUMERICAL METHOD

The governing equations correspond to an incompressible, constant viscosity flow, that is

$$\rho\frac{\partial u}{\partial t} + \rho(u\cdot\nabla)u - div\ (2\mu Du) + \nabla p = f, \qquad div\ u = 0 \tag{1}$$

where u is the velocity field, ρ the density, μ the dynamic viscosity, D the symmetric gradient operator, i.e., $(Du)_{ij} = (u_{i,j}+u_{j,i})/2$, p the pressure, and f the volumetric forces. These equations are assumed to hold in a bounded domain Ω, with initial solenoidal conditions for u in Ω, imposed velocities on the Dirichlet boundary Γ_D, and imposed tractions on the Neumann boundary Γ_N ($\overline{\Gamma_D \cup \Gamma_N} = \partial\Omega$), $\Gamma_D \cap \Gamma_N = \emptyset$).

$$u(x,0) = u_0(x)\ \forall\ x\ \in\ \Omega, \qquad u(x,t) = g(x,t)\ \forall\ x\ \in\ \Gamma_D, \qquad (-p\,\mathbf{1} + 2\mu Du)\cdot\mathbf{n} = \mathcal{F}\ \forall\ x\ \in\ \Gamma_N \tag{2}$$

Let now $\mathcal{T}_h$ be a finite element partition of Ω, and let $V_h \subset H^1(\Omega)^{n_{sd}}$ be an associated finite element space to approximate the velocity field, where n_{sd} is the number of space dimensions. We assume that V_h consists of piecewise linear, bilinear or trilinear vector fields. We define, as usual,

$$V_{hD} = \{v_h\ \in\ V_h,\ v_h = g\ on\ \Gamma_D\}, \quad V_{h0} = \{v_h\ \in\ V_h,\ v_h = 0\ on\ \Gamma_D\} \tag{3}$$

and let $Q_h \subset L^2(\Omega)$ be a finite element space for the pressure. Of most interest to us is the case when the interpolants for the pressure coincide with those used for each component of the velocity field. Finally, let G_h be another vector finite element space, that we take in general coincident with V_h (no boundary conditions imposed). The SPGP method considered thus reads:[7] *Find* $(u_h^n, p_h^n, g_h^n) \in V_{hD} \times Q_h \times G_h$ *such that*

$$\left(\rho\frac{u_h^n - u_h^{n-1}}{\Delta t} + \rho(u_h^* \cdot \nabla)u_h^n, v_h\right) + a(u_h^n, v_h) - (p_h^n, div\ v_h) - (f, v_h) - \int_{\Gamma_N} \mathcal{F} \cdot v_h\ d\Gamma +$$

$$+ \sum_{K\,\in\,\mathcal{T}_h} \left(\rho\frac{u_h^n - u_h^{n-1}}{\Delta t} + \rho(u_h^* \cdot \nabla)u_h^n + \nabla p_h^n - f, \frac{\tau_u}{\rho}[\rho(u_h^* \cdot \nabla)v_h]\right)_K = 0 \qquad (4)$$

$$(q_h, div\ u_h^n) + \sum_{K\,\in\,\mathcal{T}_h} \left(\nabla p_h^n - g_h^{n-1+\beta}, \frac{\tau_p}{\rho}\nabla q_h\right)_K = 0 \qquad (5)$$

$$(-\nabla p_h^n + g_h^n, \xi_h) = 0 \qquad (6)$$

for all $(v_h, q_h, \xi_h) \in V_{h0} \times Q_h \times G_h$. In (4), $a(\cdot,\cdot)$ is the viscous bilinear form, u_h^* can be taken as u_h^n or u_h^{n-1}, the latter corresponding to the standard linearized treatment of convection, and τ_u is the SUPG intrinsic time

$$\tau_u = \frac{\alpha(Re_K)h_K}{2 \mid u^{n-1} \mid}, \quad Re_K = \frac{\rho \mid u^{n-1} \mid h_K}{12\mu}, \quad \alpha(Re_K) = \min(1, Re_K) \qquad (7)$$

and τ_p is a second intrinsic time. In Ref.[7] the value $\rho h_K^2/(12\mu)$, differing just by a factor of two from the low-Reynolds formula for τ_u is adopted. In practice this value is slightly too large for high-Reynolds computations, a better choice being $\tau_p = \tau_u$. Simpler formulae for the stabilization parameters were proposed by Codina.[4] Notice that the previous formulation is of the backward Euler kind, except for the appearance of $g_h^{n-1+\beta}$ if $\beta < 1$. For the algorithmic cost to be competitive, the choice $\beta = 0$ is mandatory. The matrix formulation of (4)-(6) is

$$\frac{1}{\Delta t}\mathbf{M}_U(\underline{U}^n - \underline{U}^{n-1}) + (\mathbf{A} + \mathbf{K})\underline{U}^n - \tilde{\mathbf{B}}\underline{P}^n = \underline{F} \qquad (8)$$

$$\mathbf{B}^T\underline{U}^n + \frac{1}{\rho}\mathbf{L}\underline{P}^n - \frac{1}{\rho}\mathbf{D}^T\underline{G}^{n-1+\beta} = \underline{0} \qquad (9)$$

$$-\mathbf{C}\underline{P}^n + \mathbf{M}\underline{G}^n = \underline{0} \qquad (10)$$

where $\underline{U}^n$, $\underline{P}^n$ and $\underline{G}^n$ are the vectors containing the unknowns, $\mathbf{M}_U$, $\mathbf{A}$ and $\mathbf{K}$ are the matrices arising from the temporal derivative, convective and viscous terms, respectively (including the stabilization terms), and

$$\mathbf{B}_{IJ} = \int_\Omega M^J div\ N^I\ d\Omega, \qquad \tilde{\mathbf{B}}_{IJ} = \mathbf{B}_{IJ} - \int_\Omega \tau_u \nabla M^J \cdot (u_h^n \cdot \nabla)N^I\ d\Omega, \qquad (11)$$

$$\mathbf{D}_{IJ} = \int_\Omega \tau_p \nabla M^J \cdot N^I\ d\Omega, \qquad \mathbf{C}_{IJ} = \int_\Omega \nabla M^J \cdot N^I\ d\Omega, \qquad (12)$$

$$\mathbf{L}_{IJ} = \int_\Omega \tau_p \nabla M^J \cdot \nabla M^I\ d\Omega, \qquad \mathbf{M}_{IJ} = \int_\Omega M^J M^I\ d\Omega \qquad (13)$$

M^I and N^I being, respectively, the I-th basis function for pressure and velocity (N^I is, thus, vectorial). The mass matrix $\mathbf{M}$ can be used in consistent form or lumped form.

FOURIER ANALYSIS OF THE STEADY STATE

To perform the Fourier analysis, a model 1D problem is introduced that retains the main features of the Navier-Stokes equations. We keep the notation u and p for the unknowns to make the analogy evident. The proposed equations are

$$\rho\frac{\partial u}{\partial t} + \rho u\frac{\partial u}{\partial x} - 2\mu\frac{\partial^2 u}{\partial x^2} + \frac{\partial p}{\partial x} = f, \qquad \frac{\partial u}{\partial x} = 0 \qquad (14)$$

Let us omit the SUPG terms ($\tau_u = 0$) and linearize the problem replacing the nonlinear term $\rho u \frac{\partial u}{\partial x}$ by $\rho c \frac{\partial u}{\partial x}$. The SPGP method, with $\mathbf{M}$ lumped and assuming f continuous and piecewise linear, leads to the following stencil

$$\begin{aligned} \frac{\rho}{6\Delta t}\left(U_{i-1}^n + 4U_i^n + U_{i+1}^n - U_{i-1}^{n-1} - 4U_i^{n-1} - U_{i+1}^{n-1}\right) + \\ +\rho c\frac{U_{i+1}^n - U_{i-1}^n}{2h} - 2\mu\frac{U_{i+1}^n - 2U_i^n + U_{i-1}^n}{h^2} + \frac{P_{i+1}^n - P_{i-1}^n}{2h} &= \frac{F_{i-1}^n + 4F_i^n + F_{i+1}^n}{6} \quad (15) \\ \frac{U_{i+1}^n - U_{i-1}^n}{2h} - \frac{\tau_p}{\rho}\frac{P_{i+1}^n - 2P_i^n + P_{i-1}^n}{h^2} &= -\frac{\tau_p}{\rho}\frac{P_{i+2}^{n-1+\beta} - 2P_i^{n-1+\beta} + P_{i-2}^{n-1+\beta}}{4h^2} \quad (16) \end{aligned}$$

where h is the mesh size and capital letters denote nodal values of the unknowns. If $\tau_u > 0$, Eq. 15 is modified adding

$$-\tau_u\left\{\frac{\rho c}{\Delta t}\frac{U_{i+1}^n - U_{i-1}^n + U_{i+1}^{n-1} - U_{i-1}^{n-1}}{2h} + \rho c^2\frac{U_{i+1}^n - 2U_i^n + U_{i-1}^n}{h^2} + c\frac{P_{i+1}^n - 2P_i^n + P_{i-1}^n}{h^2}\right\}$$

to the left-hand side, and $-\tau_u c\frac{F_{i+1}-F_{i-1}}{2h}$ to the right-hand side.
The Fourier analysis of the steady state, which is restricted to Stokes flow ($\rho = 0$), roughly follows the lines of Ref.[14] Let us consider the following stencil,

$$-(2\mu+\nu)\frac{U_{i+1} - 2U_i + U_{i-1}}{h^2} + \frac{P_{i+1} - P_{i-1}}{2h} = \frac{F_{i-1} + F_i + F_{i+1}}{6} \quad (17)$$

$$\frac{U_{i+1} - U_{i-1}}{2h} - \alpha\frac{P_{i+1} - 2P_i + P_{i-1}}{h^2} + \gamma\frac{P_{i+2} - 2P_i + P_{i-2}}{4h^2} = -\delta\frac{F_{i+1} - F_{i-1}}{2h} \quad (18)$$

This stencil, with suitable values for the constants ν, α, γ and δ, corresponds to the steady state formulation of the SPGP method ($U_i^n = U_i^{n-1} = U_i$, $P_i^n = P_i^{n-1} = P_i$) . It also allows for the comparison of the SPGP method ($\delta = 0$, $\alpha = \gamma$) with the GLS method ($\delta = \alpha$, $\gamma = 0$). Let now

$$\mu' = 2\mu + \nu, \quad \tilde{\alpha} = \frac{\alpha\mu'}{h^2}, \quad \tilde{\gamma} = \frac{\gamma\mu'}{h^2}, \quad \tilde{\delta} = \frac{\delta\mu'}{h^2},$$

and defining $V = \frac{U\mu'}{h^2}$, $\quad G_{i+\frac{1}{2}} = \frac{P_{i+1}-P_i}{h}$ the stencil becomes

$$\begin{aligned} -(V_{i+1} - 2V_i + V_{i-1}) + \frac{1}{2}(G_{i+\frac{1}{2}} + G_{i-\frac{1}{2}}) &= \frac{F_{i+1} + 4F_i + F_{i-1}}{6} \quad (19) \\ \frac{V_{i+1} - V_{i-1}}{2} - \tilde{\alpha}(G_{i+\frac{1}{2}} - G_{i-\frac{1}{2}}) + \frac{\tilde{\gamma}}{4}\left(G_{i+\frac{3}{2}} + G_{i+\frac{1}{2}} - G_{i-\frac{1}{2}} - G_{i-\frac{3}{2}}\right) &= -\frac{\tilde{\delta}}{2}\left(F_{i+1} - F_{i-1}\right) \quad (20) \end{aligned}$$

Assuming now that i runs from $-\infty$ to $+\infty$ and inserting Fourier modes

$$V_i \to \hat{V}e^{-Iikh}, \quad G_i \to \hat{G}e^{-Iikh}, \quad F_i \to \hat{F}e^{-Iikh},$$

with k the Fourier variable and $I = \sqrt{-1}$, and denoting $\theta = kh/2$, the following system is obtained

$$4\sin^2\theta\ \hat{V} + \cos\theta\ \hat{G} = \left(1 - \frac{2}{3}\sin^2\theta\right)\ \hat{F}, \qquad \cos\theta\ \hat{V} + \left(\tilde{\gamma}\cos^2\theta - \tilde{\alpha}\right)\ \hat{G} = -\tilde{\delta}\cos\theta\ \hat{F} \quad (21)$$

Symbolic manipulation[18] was used to get $\hat{V}$ and $\hat{G}$. Its expansions around $\theta = 0$ read

$$\begin{aligned} S_V := \frac{\hat{V}}{\hat{F}} &= \tilde{\alpha} - \tilde{\delta} - \tilde{\gamma} + \left[-4\tilde{\alpha}^2 - \frac{2}{3}\tilde{\gamma}(-1 + 6\tilde{\delta} + 6\tilde{\gamma}) + \tilde{\alpha}\left(\frac{1}{3} + 4\tilde{\delta} + 8\tilde{\gamma}\right)\right]\ \theta^2 + \mathcal{O}(\theta^4) \quad (22) \\ S_G := \frac{\hat{G}}{\hat{F}} &= 1 + \left[-\frac{1}{6} + 4(-\tilde{\alpha} + \tilde{\delta} + \tilde{\gamma})\right]\ \theta^2 + \mathcal{O}(\theta^4) \quad (23) \end{aligned}$$

Notice that the exact dependences (if $\theta \neq 0$) are $\hat{V} = 0$, $\hat{G} = \hat{F}$, or, in other terms, $S_V = 0$ and $S_G = 1$. For the scheme to coincide with these values at $\theta \to 0$ the only condition is $\tilde{\alpha} - \tilde{\gamma} - \tilde{\delta} = 0$. Both the GLS and the SPGP methods satisfy this condition. Let us impose thus $\tilde{\gamma} = \tilde{\alpha} - \tilde{\delta}$. In this case,

$$S_V = \left(\tilde{\alpha} - \frac{2}{3}\tilde{\delta}\right)\ \theta^2 + \mathcal{O}(\theta^4), \qquad S_G = 1 - \frac{\theta^2}{6} + \mathcal{O}(\theta^4)$$

From this we learn, on the one hand, that asymptotic accuracy (as $kh \to 0$) cannot be improved beyond second order (which is the expected spatial accuracy), as S_G is second order accurate for any choice of $\tilde{\alpha}$ and $\tilde{\delta}$. On the other hand, accuracy in the velocity could be improved by choosing a linear combination of the GLS and SPGP methods, namely $\tilde{\alpha} = \frac{2}{3}\tilde{\delta}$ (implying $\tilde{\gamma} = -\frac{1}{3}\tilde{\delta}$). The gain is however not significant, since in general accuracy in velocity is much higher than in pressure.

The selection of $\tilde{\alpha}$ and $\tilde{\delta}$ must be made examining the accuracy when kh is far away from zero, as the behavior in the vicinity of zero does not depend on these parameters. We have focused on two cases: GLS ($\tilde{\alpha} = r$, $\tilde{\delta} = r$, $\tilde{\gamma} = 0$) and SPGP ($\tilde{\alpha} = r$, $\tilde{\gamma} = r$, $\tilde{\delta} = 0$). Comparison is made for $r = 10^{-1}$, 10^{-2} and 10^{-3}. Plots of S_G vs. θ can be seen in Figs. 1 and 2.

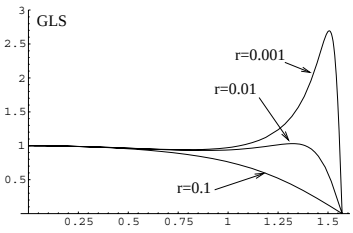

Figure 1: S_G vs. θ for GLS method with $r = 10^{-1}$, 10^{-2} and 10^{-3}.

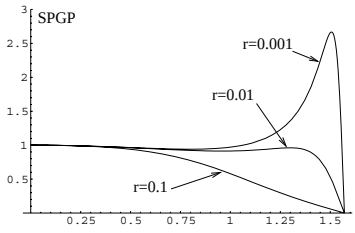

Figure 2: S_G vs. θ for SPGP method, $r = 10^{-1}$, 10^{-2} and 10^{-3}.

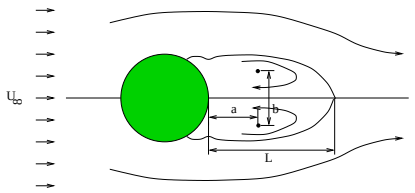

Figure 3: Problem geometry and definition of a, b and L.

By direct inspection of Figs. 1 and 2 it becomes clear that, for both the SPGP and GLS methods, $r = 10^{-2}$ is the best choice. For $r = 10^{-1}$ S_G is significantly lower than the exact value one for θ as low as 0.75. For $r = 10^{-3}$ S_G exhibits a peak near the mesh mode ($\theta = \frac{\pi}{2}$), evidencing that the Galerkin formulation is not properly stabilized. From the observation that r (and thus $\tilde{\alpha}$) must roughly be equal to 10^{-2}, since $\frac{\tau_p}{\rho} = \alpha = \frac{\tilde{\alpha}h^2}{\mu'}$ it follows that a good choice for $\frac{\tau_p}{\rho}$ is $\frac{\tau_p}{\rho} = \frac{h^2}{100\mu'}$ for both methods, which is consistent with usual adopted formulae for GLS.[11]

START-UP FLOW: SPURIOUS PRESSURE WAVE

To motivate the von Neumann's analysis of the next section, we briefly report here on a numerical test. The problem consists of the start-up flow around a circular cylinder at $Re = 3000$, defined as $Re = \rho U_\infty D/\mu$, U_∞ being the unperturbed flow velocity and D the cylinder's diameter. The domain is $\Omega = (-5, 15) \times (-5, 5) \setminus C$, with C the cylinder of unit diameter centered at the origin. This problem has been studied both experimentally[1] and numerically.[17] Starting from rest, U_∞ is impulsively modified to $U_\infty = 1$, with $D = 1$, $\rho = 3000$ and $\mu = 1$. The flow is characterized by the formation and growth of two main symmetric vortices downstream of the cylinder, with some secondary vortices also appearing (see Fig. 3). The simulation time is 3 units, with a time step of $\Delta t = 0.001$. Numerical parameters were: τ_u according to (7), $\tau_p = \tau_u$, $\beta = 0$. The mesh consisted of 11518 P_1 triangles, refined near the cylinder. The main fact is that the velocity field is accurately predicted. In Fig. 4 a quantitative comparison of the time evolution of a, b and L with experiment is shown.

The behavior of the pressure is quite surprising. A typical evolution of the pressure at a point in the domain is shown in Fig. 5. A spurious oscillation is observed, roughly a sinusoidal function with decaying amplitude. This is associated to a long-wavelength, quasi-1D wave, that can be seen in Fig. 6 at time $t = 0.4$. This wave persists for approximately 1 time unit and is superposed to the correct pressure field, though it does not affect the velocity field since its gradient is small. The decay time is empirically seen to be almost independent of Δt. This numerical artifact motivated the von Neumann analysis reported in the next section. It should be kept in mind, however, that for less severe transients

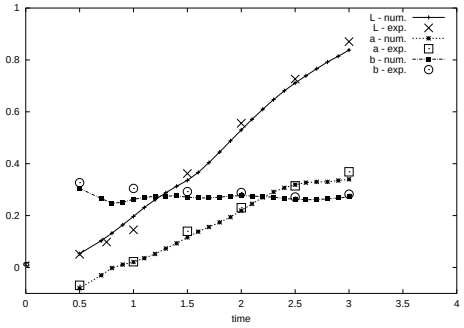

Figure 4: Comparison of numerically obtained time evolution of L, a and b to experimental data.

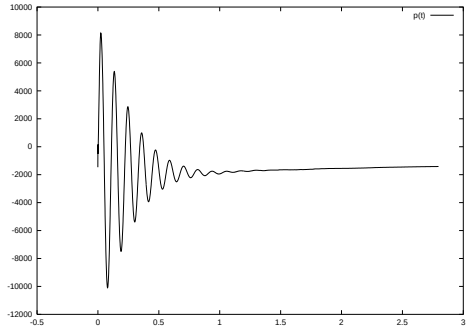

Figure 5: Typical evolution of pressure at a point.

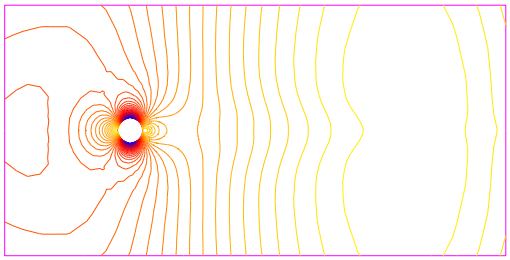

Figure 6: Pressure field at time $t = 0.4$. Notice the spurious wave, with wavelength of the order of the domain size.

no spurious wave appears. Vortex shedding at $Re = 100$, 200 and 400, e.g., is accurately simulated.

VON NEUMANN'S ANALYSIS OF THE TRANSIENT CASE

Stability analysis

The stability of the SPGP method has been addressed by Codina and Blasco in[7] for the Navier-Stokes problem using variational methods. We address here the stability analysis of the SPGP method for the model 1D problem (14) using von Neumann's technique. The advantage of this simplified setting (linear, 1D, domain $= (-\infty, +\infty)$) is that it is possible to scrutinize the algorithm's temporal behavior, but of course the assumption that the Navier-Stokes problem will behave alike is not rigorous. However, in next paragraphs we show some evidence in this direction.

Consider the stencil (15)-(16). It corresponds to the SPGP method as analyzed in Ref.[7] After the substitution $U_i^n \rightarrow Ar^n e^{-Iikh}$, $P_i^n \rightarrow Br^n e^{-Iikh}$ (r is now the *amplification factor*) we obtain a homogeneous linear system of two algebraic equations for the two unknowns A and B. To avoid trivial solutions the determinant of the system must vanish. This condition provides a relation between r and the six free parameters $\Delta t, h, c, \rho, \mu, k$, from which the two eigenvalues (denoted r_1 and r_2) were obtained by symbolic manipulation using *Mathematica*.[18] The number of parameters can be reduced to three, the mesh Reynolds number, $Re_h = \rho ch/\mu$, the *CFL* number, $C = c\Delta t/h$ and the nondimensional wavenumber $\kappa = kh$.

By inspection of *Mathematica*'s plots, and as predicted in Ref.,[7] the SPGP method is stable ($|r| < 1$) both for $\beta = 0$ and $\beta = 1$. Graphs of $|r| := \max\{|r_1|, |r_2|\}$ for the case $\beta = 0$ are shown in Fig. 7 (a) and (b). Part (a) corresponds to $Re_h = 0.01$, and three values of C are considered: 0.05, 0.5 and 5. The same is done in part (b) for $Re_h = 100$. Due to the incompressibility constraint (in 1D), both eigenvalues r_1 and r_2 are zero in the exact problem for any $k > 0$. This means that waves of finite wavelength are instantaneously damped and only uniform (rigid) motions are allowed. However, $|r|$ is not zero in the discrete problem as shown in the graphs. In general the eigenvalues are complex, so that the uniform motion is reached after a spurious oscillatory transient in which decaying waves are observed. For low Re_h and waves with $kh \sim 2$ the amplitude is multiplied by ~ 0.1 each time step. Long waves $kh \sim 0$ become more persistent as *CFL* decreases. This spurious behavior aggravates in the high-Re_h regime. Both long and short waves become very persistent ($|r| \sim 1$) for small *CFL*. In Fig. 8 the typical decay time τ of long

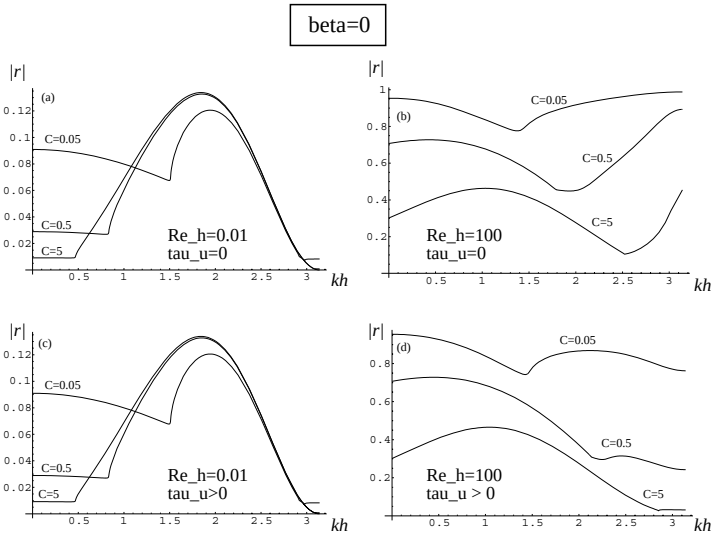

Figure 7: Amplification factor of the SPGP method for the case $\beta = 0$. Two values of Re_h are considered (0.01 and 100), and three values of the *CFL* number ($C = 0.05$, 0.5, 5). Treatment of the momentum equation: (a) and (b) Galerkin, (c) and (d) SUPG.

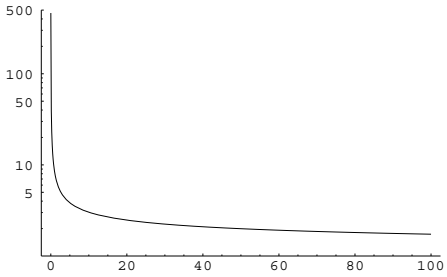

Figure 8: Long waves ($k = 0$). $\frac{\tau}{\Delta t}$ vs. Courant's number. ($\frac{\tau}{\Delta t}$ is independent on the Reynolds number.) SPGP method, $\beta = 0$, no upwinding.

waves relative to Δt is shown as a function of *CFL* (for such long waves $|r|$ is independent of Re_h, τ is defined as the time elapsed before the amplitude of the wave reduces to 1 % of its initial value). Notice that $\frac{\tau}{\Delta t} \to \infty$ as *CFL* $\to 0$. This phenomenon constitutes a remarkable spurious temporal behavior of the the SPGP method with explicit treatment of the pressure gradient projection ($\beta = 0$). No such behavior is found, as shown later on, if the pressure gradient projection is dealt with implicitly ($\beta = 1$) or if GLS or Chorin's stabilization techniques are used, since in these cases $|r| \to 0$ when $kh \to 0$.

Figs. 7 (c) and (d) show the effect of adding SUPG stabilization to the momentum equation. The low-Re_h regime remains the same as expected. For high Re_h the damping of short waves ($kh \sim \pi$) is increased, but no improvement is brought to long-wave damping. It has to be remarked that convection must be taken into account in the design of τ_p. In fact, if the expression $\tau_p = \frac{\rho h^2}{12\mu}$ used in[7] (based on the viscous-dominated case) is adopted, the situation gets worse.

One concludes that, though the SPGP method with $\beta = 0$ is indeed stable , spurious transients appear that may pollute the results during many time steps, especially in those regions of the domain where the *CFL* is smallest (because of larger mesh size or smaller velocity). Notice that this already explains the spurious behavior of the previous section. In fact, far from the cylinder we had $h \sim 0.3$ leading to $Re_h \sim 900$ and $C \sim 0.003$, values that fall well within the range of long-wave persistence.

As said above, let us now show that this phenomenon is linked to the choice $\beta = 0$. In Fig. 9 we show similar plots for $\beta = 1$. SUPG stabilization has been applied to the momentum equation to damp the short waves (velocity wiggles). In the low-Re_h regime all wavelengths are strongly damped ($|r| < 0.01$). For high Re_h and low *CFL* some persistence of waves in the range $0.1 < kh < \pi$ is predicted, but $|r|$ is small enough ($|r| \sim 0.8$ or lower) to damp perturbations after a few (~ 30) time steps.

A cure for long spurious transients is thus to take $\beta = 1$. This is however not practical since the computational cost becomes prohibitive. An alternative may come from extrapolation. We have considered two possibilities:

$$\text{EXTRAP1:} \qquad \mathbf{D}^T\mathbf{M}^{-1}\mathbf{C}\underline{P}^n \sim \mathbf{D}^T\mathbf{M}^{-1}\mathbf{C}(2\underline{P}^{n-1} - \underline{P}^{n-2})$$

$$\text{EXTRAP2:} \qquad \mathbf{D}^T\mathbf{M}^{-1}\mathbf{C}\underline{P}^n \sim 2\mathbf{D}^T\mathbf{M}^{-1}\mathbf{C}\underline{P}^{n-1} - \mathbf{L}\underline{P}^{n-2}$$

Unfortunately, both are unstable. Plots of $|r|$ show that, irrespective of Re_h and C, there exist waves with $|r| > 1$. In agreement with these predictions, when these extrapolation schemes were coded exponential instability was found.

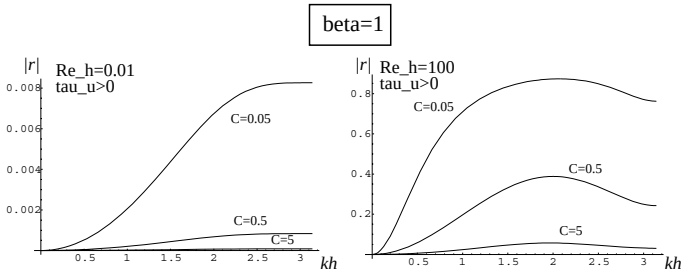

Figure 9: Amplification factor of the SPGP method for the case $\beta = 1$. Two values of Re_h are considered (0.01 and 100), and three values of the CFL number ($C = 0.05,\ 0.5,\ 5$). Treatment of the momentum equation: SUPG.

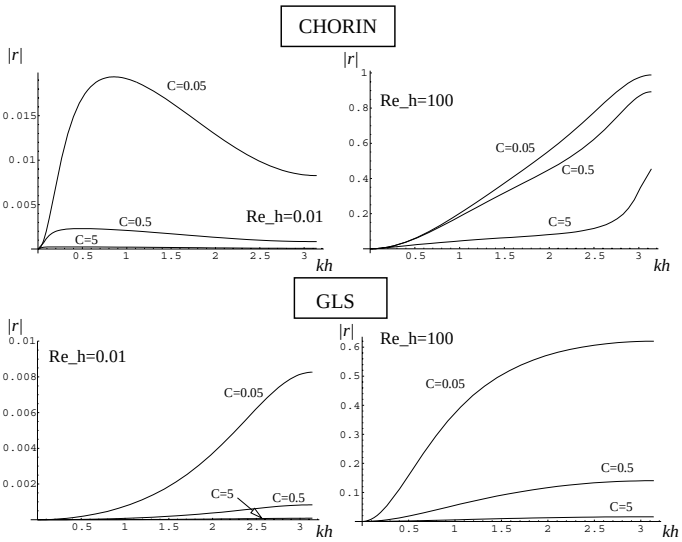

Figure 10: Amplification factor of Chorin's and GLS methods. Two values of Re_h are considered (0.01 and 100), and three values of the CFL number ($C = 0.05,\ 0.5,\ 5$).

Comparison to GLS and Chorin's methods

It is interesting to compare the results above to those corresponding to GLS and Chorin's methods. The amplification factors $|r|$ for these methods are plotted as functions of kh for high-Re and low-Re regimes in Fig. 10. Both have $|r| \to 0$ as $kh \to 0$. Both are stable and lead to some (in fact small) persistence of waves only if Re_h is large and C small, as does the SPGP method with $\beta = 1$. Least prone to this phenomenon is Chorin's method (the short waves with $kh \sim \pi$ can be damped introducing upwinding in the momentum equation, which was not done). The predictions are however comparable for the three methods.

One more variant: Stabilization by residual projection

The SPGP method, in the case of Stokes flow, can be regarded as a modification of the GLS method. The only difference is that the projection of the residual, $\Pi_h \mathcal{R}$, onto V_h is subtracted from the residual itself within the stabilization term. Consistency is not lost, since for the exact solution the residual vanishes. With this interpretation one could proceed analogously for the transient Navier-Stokes problem, arriving at a variant of the SPGP method. In this case the residual is

$$\mathcal{R}(u_h, p_h) = \rho \frac{\partial u_h}{\partial t} + \rho(u_h \cdot \nabla)u_h - 2div\ (\mu D u_h) + \nabla p_h - f \tag{24}$$

For non-zero Re the residual of the incompressibility constraint also enters the GLS formulation,[10] times a mesh-dependent constant $\delta_K = \rho\ |u|^2 \tau_u$ and thus, assuming linear elements, the stabilization terms are

$$\sum_{K \in \mathcal{T}_h} \left((\rho(u_h \cdot \nabla)u_h + \nabla p_h) - \Pi_h(\rho(u_h \cdot \nabla)u_h + \nabla p_h), \frac{\tau_u}{\rho}(\rho(u_h \cdot \nabla)v_h + \nabla q_h) \right)_K +$$

$$+ \sum_{K \in \mathcal{T}_h} \delta_K \left(div\ u_h - \Pi_h div\ u_h, div\ v_h \right)_K \qquad (25)$$

An almost equivalent formulation is proposed in,[5] where it is shown that it is in fact a sub-grid scale method[13] with a particular choice for the space of sub-scales. Von Neumann's analysis of this method yields results that resemble those of the SPGP method. In this case the possibility also appears of dealing with the residual projection either implicitly ($\beta = 1$ in the SPGP method) or explicitly ($\beta = 0$), and again the only reasonable choice (from the computational point of view) is the latter. The results are not shown here for lack of space.

NUMERICAL TESTS

The predictions of the previous section are based on the linearized version of the model problem (14), disregarding boundary effects. We now check that the conclusions are not overruled as soon as these simplifying hypotheses are dropped.

Comparison on a 1D model problem

Considering first the full (nonlinear) 1D model problem (14), to be solved for $t > 0$ in $\Omega = (0, 1)$ with $f = 0$ and initial and boundary conditions $u(x, t = 0) = 0$, $u(0, t > 0) = 1$, $p(1, t > 0) = 0$. The exact solution is $u(x, t) = 1, \quad p(x, t) = 0$.

A series of numerical experiments on this problem were performed using the SPGP method. Linear 1D finite elements were used. Experiences were made with $\rho = 1$, $\mu = 1/45000$, for different values of h and Δt. The computed pressure is seen to oscillate around zero with an amplitude that decays to zero. This is a spurious pressure transient that is activated by the sudden imposition of $u = 1$ on the left boundary. The period of the oscillations, and the decay behavior, are not predictable *a priori* due to the nonlinearity of the problem. Our aim here is to compare them with the predictions from von Neumann's analysis (that rigorously apply just to the linearized model with no boundary).

In Fig. 11 we present results for some selected cases. Plotted is the pressure at $x = 0$. The solid lines correspond to the numerical experiments and the dashed ones to von Neumann's analysis predictions. To be precise, the dashed lines correspond to (the real part of) the functions

$$u(x = 0, n\Delta t) = Ar^n, \qquad p(x = 0, n\Delta t) = Br^n$$

where r is the amplification factor of the method. As von Neumann's analysis does not predict the initial magnitudes and phases of u and p (i.e., A and B), these have been adjusted so that they coincide with the numerical result at the first positive peak. The value of r was obtained with Mathematica for the values of h, Δt, μ and ρ used in each simulation. The wavenumber k was assigned the value zero, since long waves are the most persistent ones for the cases considered, and c was set to one.

The values of Δt and h are shown in the inserts of each graph. Except for a short initial transient (probably dominated by nonlinear effects), the computed pressure exhibits practically the same temporal behavior as the one predicted by von Neumann's analysis. Both the oscillation period and the decay time are in good agreement. This supports the use of the results of the previous section to draw conclusions about the temporal behavior of the SPGP method in a broader class of cases than that to which the von Neumann's analysis rigorously applies.

Comparison to 2D start-up flow results

Finally, let us analyze the more interesting situation of the two-dimensional start-up flow around a cylinder solved by finite elements, as described in Section . Parameters for this case were taken from the 2D problem: $h = 0.3$, $C = \frac{c\Delta t}{h} = 3.33 \times 10^{-3}$, $Re_h = 900$. As in this case we have again a high Re_h and a low C, von Neumann's analysis predicts that the most persistent wave would correspond to $k = 0$. In Fig. 12 the full line represents the computed pressure value behind the cylinder. The dashed line is the real part of Ar^n, with $n = \frac{t}{\Delta t}$ and r being the amplification factor corresponding to the parameters listed above. This time, the continuous and dashed curves were put into coincidence (by adjusting A) at the second positive peak because during the first period of the simulation a second mode can be observed, superimposed to the most persistent, long-wave one.

It can be appreciated that both extinction time and period of oscillation compare well to (though being slightly larger than) those of the finite element calculation. In spite of the differences between both situations (2D vs. 1D, nonlinearity vs. linearity, irregular vs. regular meshes, etc.), the coincidences are remarkable. The simple model captures the basic features of this spurious wave phenomenon.

CONCLUDING REMARKS

A detailed Fourier analysis and several numerical tests have been reported on the recent SPGP method. These complement and extend previous theoretical results by Codina and Blasco.[7] Unconditional stability is predicted, irrespective of the choice of β. SUPG treatment of the momentum equation has no deleterious effect on stability and damps, as expected, velocity wiggles. In fact, a better choice of the stabilization parameter τ_p is the SUPG intrinsic time τ_u as given by expression (7). An alternative way of incorporating convection in the design of the intrinsic time can be found in Ref.[4]

Numerical tests on start-up flow around a cylinder at $Re = 3000$ show that the velocity field is accurately predicted. However, a spurious pressure transient pollutes the pressure field during about half of the simulated time. This phenomenon, not previously reported, should be considered when using the SPGP method for, e.g., drag calculations or fluid-structure interaction, where accuracy in the pressure field is needed. Less demanding calculations such as vortex shedding have not shown this problem.

Fourier analysis identifies these spurious transients as coming from explicit treatment of the pressure gradient projection ($\beta = 0$). It is predicted to be most critical when Re_h is large and CFL small. This situation is typical of regions within the computational domain where the mesh is coarse or the velocity small (stagnant regions). No cure was found by means of extrapolation, since the scheme becomes unstable.

Finally, it should be remarked that all predictions coming from Fourier analysis made above do not account for finite domain size and boundary conditions. Notice that trigonometric functions are not eigenfunctions of the exact problem in bounded domains unless periodicity is assumed. Heuristically, our approach has been to draw conclusions from the infinite-domain case and consider them applicable to more realistic situations. The numerical tests reported in the previous sections (especially those in Fig. 11) support our approach, as remarkable coincidences between the predictions from von Neumann's analysis and actual computations have been obtained.

ACKNOWLEDGMENTS: This work was partially supported by Agencia Nacional de Promoción Científica y Tecnológica through grants PICT97 No. 12-00000-00982 and PMT-PICT 0392, BID 802/OC.

References

[1] R. Bouard and M. Coutanceau, *J. Fluid Mech.*, **101**, 583-607 (1980).

[2] G. Buscaglia and P. Carrica, unpublished results.

[3] A. J. Chorin, *Math. of Comp.*, **22**, 745-762 (1968).

[4] R. Codina, "A stabilized finite element method for generalized stationary incompressible flows", submitted (1998).

[5] R. Codina, "Stabilization of incompressibility and convection through orthogonal sub-scales in finite element methods", submitted (1999).

[6] R. Codina and J. Blasco, *Comp. Meth. Appl. Mech. and Eng.*, **143**, 373-391 (1997).

[7] R. Codina and J. Blasco, *Fourth World Congress on Computational Mechanics*, Buenos Aires, 1998.

[8] R. Codina and J. Blasco, "Analysis of a finite element approximation of the stationary Navier-Stokes equations using equal velocity-pressure interpolation", Publication CIMNE No. 113, May 1997, Int. Center for Numer. Meth. Eng., Barcelona.

[9] S. Felicelli, "Métodos de elementos finitos de igual orden para las ecuaciones de Navier-Stokes", CNEA-CAB Report No. 3519, Bariloche, Argentina, December 1993 (In Spanish).

[10] L. Franca and S. Frey, *Comp. Meth. Appl. Mech. Eng.*, **99**, 209-233 (1992).

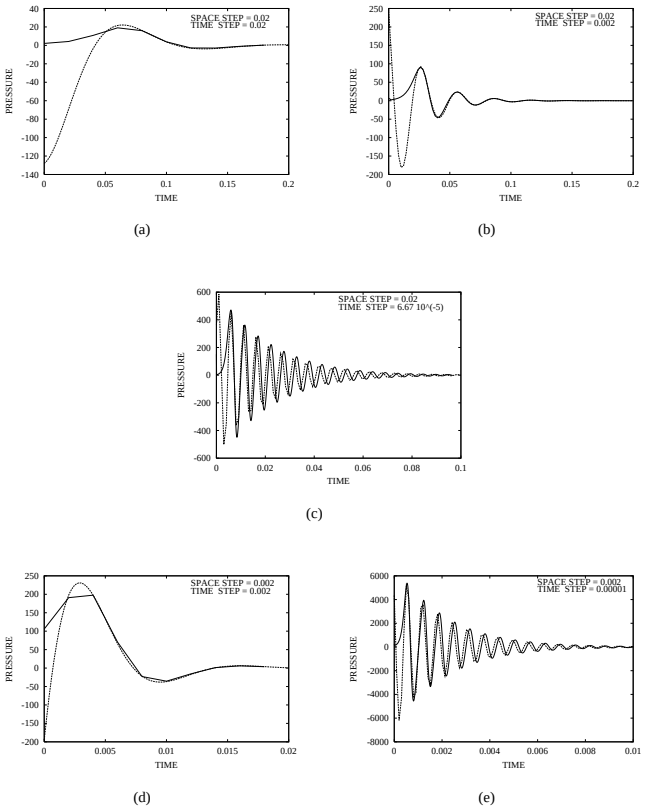

Figure 11: Pressure at $x = 0$ vs. time. Numerical experiments with the explicit SPGP method in the unit 1D interval ($\rho = c = 1$, $\mu = \frac{1}{45000}$). Solid: numerical experiment; dashed: theoretical prediction.

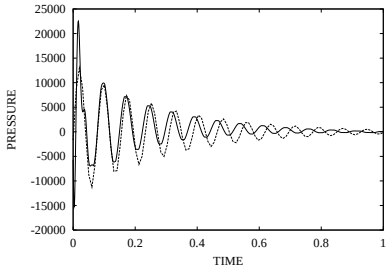

Figure 12: Start-up flow around a cylinder. Pressure behind the cylinder vs. time. A comparison with theoretical 1D predictions (dashed line). Both curves have been made to coincide at the second positive peak.

[11] L. Franca, T. Hughes and R. Stenberg, "Stabilized finite element methods", in *Incompressible Computational Fluid Dynamics*, M. Gunzburger and R. Nicolaides (Eds.), Cambridge Univ. Press, 1993. **23**, 423-453 (1991).

[12] W. Habashi, M. Peeters, M. Robichaud and V.-N. Nguyen, in *Incompressible Computational Fluid Dynamics*, M. Gunzburger and R. Nicolaides (Eds.), Cambridge Univ. Press, 1993.

[13] T. Hughes, *Comp. Meth. Appl. Mech. Eng.*, **127**, 387-401 (1995).

[14] S. Idelsohn, M. Storti and N. Nigro, *Int. J. Numer. Meth. in Fluids*, **20**, 1003-1022 (1995).

[15] A. Lew. Master's Thesis in Nuclear Engineering, Instituto Balseiro, 1998.

[16] A. Lew, G. Buscaglia and P. Carrica, "A robust equal-order finite element formulation for the k-epsilon turbulence model", submitted.

[17] T. Tanahashi and H. Okanaga, *Int. J. Numer. Meth. Fluids*, **11**, 479-499 (1990).

[18] S. Wolfram, *Mathematica*, 2nd edition, Addison-Wesley, 1991.

[19] O. C. Zienkiewicz and R. Codina, *Int. J. Numer. Meth. Fluids*, **20**, 869-885 (1995).